IOP PUBLISHING LASER PHYSICS
Laser Phys. **23** (2013) 015201 (12pp) doi:10.1088/1054-660X/23/1/015201

Theory of cavity-enhanced spontaneous four wave mixing

K Garay-Palmett[1], Y Jeronimo-Moreno[2] and A B U'Ren[1]

[1] Instituto de Ciencias Nucleares, Universidad Nacional Autónoma de México, Apartado Postal 70-543, Distrito Federal, 04510, Mexico
[2] Instituto de Física, Universidad Nacional Autónoma de México, Apartado Postal 70-543, Distrito Federal, 04510, Mexico

E-mail: karina.garay@nucleares.unam.mx

Received 15 November 2011, in final form 10 December 2011
Published 20 November 2012
Online at stacks.iop.org/LP/23/015201

Abstract
In this paper we study the generation of photon pairs through the process of spontaneous four wave mixing (SFWM) in a $\chi^{(3)}$ cavity. Our key interest is the generation of photon pairs in a guided-wave configuration—fiber or waveguide—where at least one of the photons in a given pair is matched in frequency and bandwidth to a particular atomic transition, as required for the implementation of photon–atom interfaces. We present expressions, along with plots, for the two-photon joint intensity both in the spectral and temporal domains. We also present expressions for the absolute brightness, along with numerical simulations, and show that the presence of the cavity can result in a flux enhancement relative to an equivalent source without a cavity.

(Some figures may appear in colour only in the online journal)

1. Introduction

Photon pair generation can be accomplished through spontaneous parametric processes including spontaneous parametric downconversion (SPDC), based on a second-order nonlinearity, and spontaneous four wave mixing (SFWM), based on a third-order nonlinearity. Both of these processes are extremely versatile in terms of the resulting properties which emitted photon pairs can have. Thus, SFWM has been used, or proposed, as the basis for the generation of factorable photon pairs [1–6], of photon pairs with arbitrary spectral correlation properties [7–9], of polarization-entangled photon pairs [10–12], and of ultrabroadband photon pairs [13]. In addition, if implemented in a fiber, SFWM has a number of important advantages including the possibility of very long interaction lengths and straightforward integration with existing fiber optic networks. Recently, in the context of classical optics there have been important experimental demonstrations of four wave mixing (FWM) [14] and the implementation of nonlinear optical devices, such as wavelength converters and multi-wavelength fiber lasers, which are based on FWM [15–19]. While the use of a guided-wave configuration constrains the transverse spatial properties of emitted photon pairs, the spectral properties can vary widely. In common with SPDC, in the process of SFWM the energy splitting ratio in a given photon pair is governed only by phasematching, so that while the emission bandwidth can vary greatly in accordance with the properties of the nonlinear material and the pump, this bandwidth cannot typically be made naturally very small. In this paper we explore the use of $\chi^{(3)}$ cavities for the generation of SFWM photon pairs which are sufficiently narrowband for the effective implementation of atom–photon interfaces, i.e. so that one photon from a SFWM photon pair may be reliably absorbed by a single atom. This is an important line of research which represents a route for the implementation of quantum memories [20, 21].

This paper extends to the process of SFWM a previous analysis from our group (see [22]) of cavity-enhanced SPDC [23–34]. In our earlier paper we analyzed the spectral and temporal properties of SPDC photon pairs produced in a nonlinear cavity. We showed that the use of a high-finesse cavity results in photon pair emission constrained to the narrow spectral windows defined by the cavity modes. In addition we studied how the spectral mode structure imposed by the cavity translates into a specific mode structure in

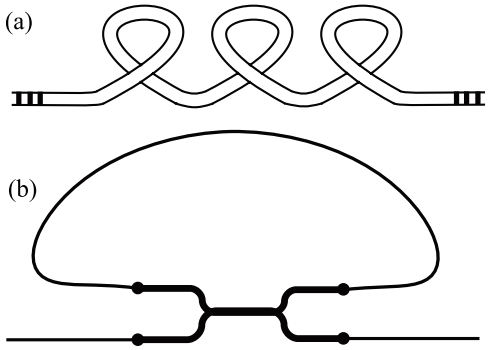

Figure 1. Two ways in which a SFWM cavity source could be implemented. In (a) two Bragg mirrors are written on a fiber, thus forming a cavity. In (b) a ring cavity (fiber- or waveguide-based) is used.

the temporal domain, and we showed that for a sufficiently narrowband pump, the presence of a cavity leads to a flux enhancement relative to an equivalent source without a cavity. In the present paper, we have carried out a corresponding analysis for SFWM. Because resonance at the emission frequencies only (i.e. excluding the pump) yields both narrowband emission modes and a cavity-induced flux enhancement, in this paper we concentrate on this case which is technologically simpler to implement. In addition, in this paper we separately analyze the cases of resonance to one or both of the emission modes. We discuss the presence of high-dimensional temporal entanglement in SFWM photon pairs emitted in a $\chi^{(3)}$ cavity, and we present an analytic expression, in closed form, for the joint temporal intensity valid under certain approximations. We present expressions for the absolute brightness along with corresponding numerical simulations, as well as a simple geometrical model which leads to an improved understanding of the cavity-induced flux enhancement.

A $\chi^{(3)}$ SFWM cavity source can be implemented with an optical fiber on which two Bragg gratings are recorded to form a cavity (see figure 1(a)). Likewise, the cavity can be in the form of a fiber ring [15–17], which could be implemented through a length of fiber connected to one input port and one output port of a fiber-based beam splitter and two lengths of fiber, to form the input and output of the device, connected to the remaining two ports (see figure 1(b)). Alternatively, recent work has shown the feasibility of observing optical nonlinear effects in waveguide micro-rings, where light is coupled and out-coupled from the cavity through a straight waveguide placed tangentially to the ring [35]. This latter route represents a highly promising approach, which could be used for generating SFWM photon pairs and which could be incorporated into integrated optics circuits. This paper aims to present the required theory for the description of various aspects of SFWM cavity sources.

2. The SFWM two-photon quantum state

In this paper we are interested in studying the spectral and temporal properties of photon pairs generated by spontaneous four wave mixing (SFWM) in a fiber-based (or waveguide-based) optical cavity. Let us begin by reviewing the SFWM two-photon state produced by a fiber, in the absence of a cavity, assuming that each of the participating modes propagates in a single transverse mode. The state which describes the signal (s) and idler (i) state produced by SFWM is given by $|\Psi\rangle = |0\rangle_s|0\rangle_i + \zeta|\Psi_2\rangle$, in terms of the vacuum $|0\rangle_s|0\rangle_i$ and the two-photon state $|\Psi_2\rangle$, where ζ is a constant related to the conversion efficiency. We have shown previously that $|\Psi_2\rangle$ is given by [6, 36]

$$|\Psi_2\rangle = \sum_{k_s}\sum_{k_i} G(k_s, k_i)\hat{a}^\dagger(k_s)\hat{a}^\dagger(k_i)|0\rangle_s|0\rangle_i, \tag{1}$$

where $\hat{a}(k_\mu)$ (with $\mu = s, i$) represents the annihilation operators for each of the signal and idler modes, labeled by the wavenumber k_μ. Expressed in terms of frequencies, the function $G(\omega_s, \omega_i)$ is the joint spectral amplitude (JSA) given by $G(\omega_s, \omega_i) = \ell(\omega_s)\ell(\omega_i)F(\omega_s, \omega_i)$ in terms of $\ell(\omega) = \sqrt{\hbar\omega/[\pi\epsilon_o n^2(\omega)]}$ and in terms of the function

$$F(\omega_s, \omega_i) = \int d\omega\, \alpha(\omega)\alpha(\omega_s + \omega_i - \omega) \times \mathrm{sinc}\left[\frac{L\Delta k(\omega_s, \omega_i, \omega)}{2}\right] e^{i\frac{L\Delta k(\omega_s,\omega_i,\omega)}{2}}. \tag{2}$$

In equation (2), L is the fiber length, $\alpha(\omega)$ represents the pump spectral envelope function and $\Delta k(\omega_s, \omega_i, \omega)$ is the phase mismatch

$$\Delta k(\omega_s, \omega_i, \omega) = k(\omega) + k(\omega_s + \omega_i - \omega) - k(\omega_s) - k(\omega_i) - 2\gamma P, \tag{3}$$

where γ and P are the nonlinear coefficient (related to self-phase and cross-phase modulation effects) and the peak pump power, respectively.

Assuming that the pump has a Gaussian spectral profile, with bandwidth σ, the coefficient ζ in equation (1) is given by

$$\zeta = i\frac{2(2\pi)^{1/2}\epsilon_0 c n(\omega_o)}{\hbar\omega_o}\frac{\gamma_{\mathrm{fwm}} LP}{\sigma}\delta k, \tag{4}$$

where ϵ_0 is the permittivity of free space, c is the speed of light, ω_o is the central frequency for the pump, and $n(\omega)$ is the refractive index of the fiber. The term γ_{fwm} is the nonlinear coefficient associated with the SFWM interaction, and δk is the mode spacing obtained in the quantization of the electromagnetic field.

2.1. Spectral-domain description of a SFWM cavity source

Let us now turn to the case where the SFWM fiber is in the form of a cavity. This could be done in one of two ways: (i) two Bragg mirrors with a separation L could be written on a length of fiber thus forming a cavity, or (ii) a fiber or waveguide ring cavity, of circulation length L_c could be used, coupled to a straight fiber or waveguide placed tangentially to the ring. In this paper we will study cases where the cavity used is resonant to one or both of the SFWM modes, while it is not resonant to the pump frequency. Figure 1 shows, schematically, both of these types of fiber

cavity sources. While we are interested in both the pulsed and continuous-wave pump regimes, we will carry out our analysis for the pulsed case and will obtain the continuous-wave case as an appropriate limit.

For simplicity, in this paper we restrict our attention to the SFWM process with degenerate pumps, i.e. for which both pump photons in a given event come from the same pump mode. In our analysis below, we will assume a cavity formed by two mirrors, although we will indicate how our results would apply to the case of a ring cavity. Because in our calculation the cavity is not resonant to the pump, as mentioned above, both mirrors are perfectly transmissive for the pump. We will refer to a fiber cavity SFWM source resonant only to the signal-photon as the Cs cavity, to a source resonant only to the idler-photon as a Ci cavity, and to a source resonant to both SFWM photons as a Csi cavity. We also assume that the left-hand cavity mirror (through which the pump enters, to be referred to as mirror 1) is perfectly reflective for SFWM photons, so that all emitted photons are forward-propagating, transmitted by the right-hand cavity mirror (to be referred to as mirror 2). The calculation below closely follows that for SPDC reported by us in an earlier paper, see [22].

For the Csi cavity it can be shown that the two-photon component of the state at the cavity output becomes

$$|\Psi_2^{si}\rangle = \zeta \sum_{k_s} \sum_{k_i} G_{si}(k_s, k_i) a_s^\dagger(k_s) a_i^\dagger(k_i) |0\rangle_s |0\rangle_i, \tag{5}$$

where we have defined the joint amplitude function

$$G_{si}(\omega_s, \omega_i) = G[k_s(\omega_s), k_i(\omega_i)] A_s(\omega_s) A_i(\omega_i), \tag{6}$$

given in terms of $G(k_s, k_i)$ (see equation (2)), but expressed here in terms of frequencies, and where the function $A_\mu(\omega)$ describes the effect of the cavity and can be written as

$$A_\mu(\omega_\mu) = \frac{t_{2\mu}}{1 - |r_{2\mu}| e^{i(2\beta_\mu + \delta_{1\mu} + \delta_{2\mu})}}. \tag{7}$$

In equation (7), $t_{2\mu}$ and $r_{2\mu} = |r_{2\mu}| e^{i\delta_{2\mu}}$ are the amplitude transmissivity and the amplitude reflectivity of the right-hand cavity mirror, respectively, while $r_{1\mu} = e^{i\delta_{1\mu}}$ is the amplitude reflectivity of the left-hand cavity mirror, for $\mu = s, i$. In equation (7), $\beta_\mu = k(\omega_\mu)L$ represents the phase acquired by photon μ in one round trip of the fiber cavity.

The cavity-modified JSA function is shown in equation (6). The corresponding cavity-modified joint spectral intensity (JSI) $S_{si}(\omega_s, \omega_i) = |G_{si}(\omega_s, \omega_i)|^2$ is given by [22]

$$S_{si}(\omega_s, \omega_i) = |F(\omega_s, \omega_i)|^2 \mathscr{A}_s(\omega_s) \mathscr{A}_i(\omega_i), \tag{8}$$

with $F(\omega_s, \omega_i)$ given by equation (2), and

$$\mathscr{A}_\mu(\omega_\mu) = \frac{|t_{2\mu}|^2}{\left(1 - |r_{2\mu}|\right)^2} \frac{1}{1 + \mathscr{F}_\mu \sin^2[\Delta_\mu(\omega_\mu)/2]}, \tag{9}$$

written in terms of the coefficient of finesse $\mathscr{F}_\mu$

$$\mathscr{F}_\mu = \frac{4|r_{2\mu}|}{\left(1 - |r_{2\mu}|\right)^2}, \tag{10}$$

and the phase factor

$$\Delta_\mu(\omega_\mu) = 2\beta + \delta_{1\mu} + \delta_{2\mu}. \tag{11}$$

Note that in the case of a ring cavity mirror 1 does not exist, while mirror 2 becomes a fiber-based beam splitter as shown in figure 1(b). The coefficient r_2 is then the amplitude associated with an intra-cavity photon remaining in the cavity in a given iteration, while the coefficient t_2 is the amplitude associated with an intra-cavity photon exiting the cavity in a given iteration. Because mirror 1 does not exist, $\delta_{1\mu}$ should be replaced with 0. Also, the fiber length L should be replaced with $L_r/2$, where L_r is the circulation length in the ring cavity.

The Airy function $\mathscr{A}_\mu(\omega_\mu)$ is formed by a sequence of equal height peaks, with width $\delta\omega_\mu$, and spectral separation, or free spectral range, $\Delta\omega_\mu$. Under the assumption that the index of refraction remains constant among different peaks, it can shown that [22]

$$\Delta\omega_\mu = \frac{\pi c}{L n_\mu}, \tag{12}$$

and

$$\delta\omega_\mu = \frac{2c}{L n_\mu \sqrt{\mathscr{F}_\mu}} = \frac{2\Delta\omega}{\pi\sqrt{\mathscr{F}_\mu}}, \tag{13}$$

where $n_\mu = n(\omega_{\mu 0})$ is the refractive index of the fiber evaluated at the central frequency of the signal and idler modes ($\mu = s, i$). Note that the cavity is resonant at frequencies at which the peaks of the Airy function appear. Thus, in order to ensure resonance at a particular frequency ω, the condition $\sin[\Delta_\mu(\omega)/2] = 0$ must be fulfilled. Also note that resonance at a given desired frequency can be achieved by adjusting the reflection phases $\delta_{1\mu}$ and $\delta_{2\mu}$.

For the case of a cavity resonant at only one of the SFWM modes, say the signal mode, the two-photon state and the JSI are given by equations (5) and (8), respectively, with $|r_{2i}| = 0$. Thus, $\mathscr{F}_i = 0$ and $\mathscr{A}_i(\omega_i) = 1$, and consequently the JSI for the Cs cavity becomes

$$S_s(\omega_s, \omega_i) = |F(\omega_s, \omega_i)|^2 \mathscr{A}_s(\omega_s). \tag{14}$$

Likewise, for a Ci cavity the JSI becomes

$$S_i(\omega_s, \omega_i) = |F(\omega_s, \omega_i)|^2 \mathscr{A}_i(\omega_i). \tag{15}$$

The spectral structure of a SFWM two-photon state obtained with a Csi cavity is illustrated in figures 2(a)–(c), for which we have assumed a photonic crystal fiber (PCF) with 0.68 μm core radius and 0.5 air-filling fraction, and we have relied on the step-index model [37]. These parameters have been chosen to achieve phasematching for a SFWM process with degenerate pumps centered at $\omega_p = 2\pi c/1.064$ μm and signal and idler modes centered at $\omega_s^o = 2\pi c/0.852$ μm and $\omega_i^o = 2\pi c/1.417$ μm, respectively. The SFWM frequencies are chosen to be considerably frequency non-degenerate, which facilitates photon pair splitting. We have assumed a fiber length of $L = 1$ cm and a pump bandwidth of $\sigma = 80$ GHz. Figure 2(a) represents the JSI without a cavity, i.e. so that $\mathscr{A}_s(\omega) = \mathscr{A}_i(\omega) = 1$. The two-dimensional Airy pattern describing the effect of the cavity is shown in figure 2(b), while figure 2(c) represents the resulting JSI

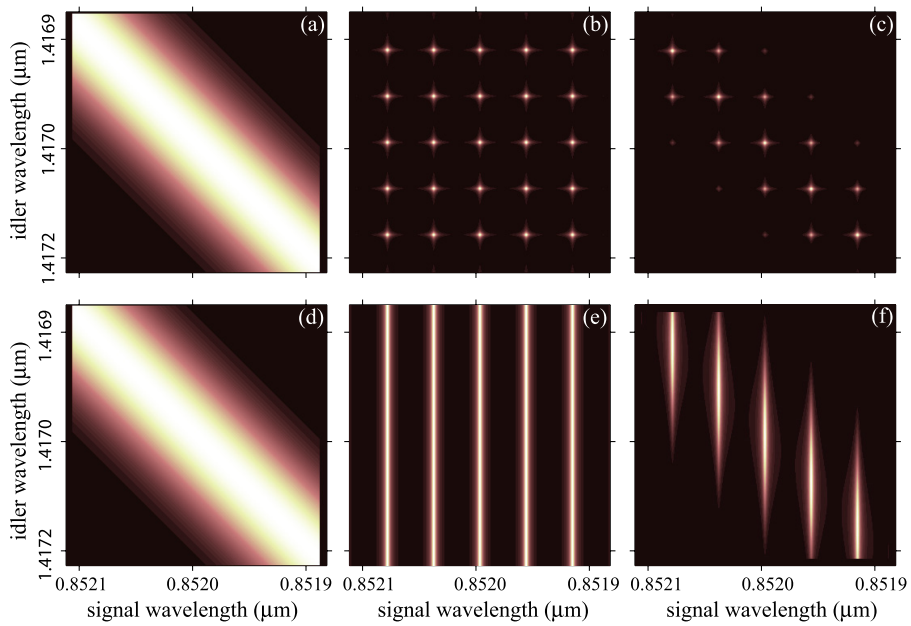

Figure 2. In this figure we show the joint spectral intensity for SFWM photon pairs produced in a $\chi^{(3)}$ cavity. In the first three panels we present, for a Csi cavity, plots prepared for a particular set of parameters (see main text), as a function of the signal and idler frequencies, of (a) the joint spectral intensity in the absence of a cavity, (b) the contribution of the cavity, comprising a matrix of cavity-allowed modes, and (c) the resulting cavity-modified joint spectral intensity. Panels (d)–(f) are similar to panels (a)–(c), except that resonance at the idler mode has been suppressed (i.e. this corresponds to the Cs cavity).

for the cavity-modified SFWM photon pairs. For illustrative purposes we have assumed here $r_2 = 0.8$, corresponding to $\mathscr{F} = 80$, in a realistic implementation the finesse would probably be chosen much higher to ensure the emission of sufficiently narrowband photon pairs. Note that for these plots (figures 2(a)–(c)), we have assumed that the signal and idler photons are filtered using rectangular filters of width $\sigma_{f\mu} = 5\Delta\omega_\mu$ (with $\mu = s, i$), centered at ω_s^o and ω_i^o, respectively.

As can be noted, the effect of the cavity is that the emission frequencies are re-distributed, with respect to the corresponding emission frequencies in the absence of a cavity, so that emission occurs only for frequencies within the cavity modes. Because the mode width $\delta\omega$ scales as $\mathscr{F}^{-1/2}$, cavity-enhanced SFWM with a sufficiently high finesse can be an effective route towards narrowband photon pairs, to be used for example in the context of atom–photon interfaces. As will be studied further in a later section, if the pump bandwidth is of the order of the cavity mode width $\delta\omega$, a significant enhancement of the source brightness can result with respect to an equivalent source without a cavity.

In figures 2(d)–(f) we illustrate the spectral structure of SFWM photon pairs produced by a Cs cavity. Here we assume an identical source configuration to that assumed for the Csi cavity, except that the resonance for the idler photon has been suppressed. figure 2(d) represents the JSI without a cavity, i.e. so that $\mathscr{A}_s(\omega) = \mathscr{A}_i(\omega) = 1$. The one-dimensional Airy pattern describing the effect of a cavity resonant for the single mode only is shown in figure 2(e), while figure 2(f) represents the resulting JSI for the cavity-modified SFWM photon pairs. As for the Csi cavity, we have assumed that the signal and idler photons are filtered using rectangular filters with width $\sigma_{f\mu} = 5\Delta\omega_\mu$, centered at ω_s^o and ω_i^o, respectively.

As may be appreciated, the effect of the cavity is a spectral re-distribution for the resonant, in this case signal, photon. The result is that the JSI is now formed by elongated modes of width $\delta\omega$ for the signal photon and a larger width determined by the cavity length and pump bandwidth for the idler photon.

2.2. *Temporal-domain description of a SFWM cavity source*

It is instructive to study the two-photon state in the temporal domain, in addition to the spectral domain used in our description so far. To this end, we define the joint temporal amplitude (JTA) $\tilde{f}(t_s, t_i)$ as the two-dimensional Fourier transform of the JSA, i.e.

$$\tilde{f}(t_s, t_i) = \mathcal{F}\{G_{si}(\omega_s, \omega_i)\}, \tag{16}$$

where $\mathcal{F}$ denotes the Fourier transform and $G_{si}(\omega_s, \omega_i)$ is given according equation (6).

The joint temporal intensity (JTI) can now be written as $S_t(t_s, t_i) = |\tilde{f}(t_s, t_i)|^2$, which when properly normalized yields the time of emission joint probability distribution.

The spectral cavity mode structure translates into a specific temporal-mode structure. In figure 3, we have shown for the same source parameters as in figure 2 the resulting JTI calculated numerically through equation (16). In physical terms, the two photons in a given pair may exit the cavity together, or may be delayed with respect to each other by a whole number of cavity round trip times. The vertical (horizontal) dotted lines indicate possible signal-mode (idler-mode) emission times, corresponding to a whole number of cavity round trip times. This results in a

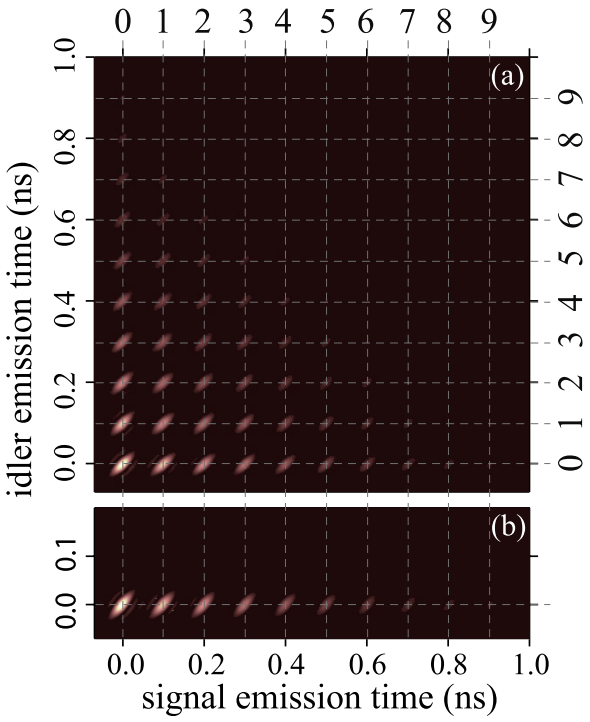

Figure 3. (a) Here we show for the same parameters as in figure 2 the joint temporal intensity for the Csi cavity, plotted as a function of the signal and idler times of emission. The vertical (horizontal) dotted lines indicate possible signal-mode (idler-mode) times of emission, each corresponding to an integer number of cavity round trips. (b) This panel is similar to panel (a), except that it has been prepared for the Cs cavity.

matrix of temporal emission modes, as is apparent in figure 3, which decay in amplitude for increasing times of emission (which imply an increasing number of cavity round trips). Of course, for a higher finesse, this amplitude roll-off is slower, resulting in the appearance of a larger number of temporal modes.

Let us label each of the emission modes according to the cavity iteration at which each of the two photons is emitted, so that the state $|ij\rangle$, with a corresponding probability amplitude C_{ij}, means the signal photon emitted in the ith cavity iteration and the idler photon emitted in the jth cavity iteration. We may then write down the resulting two-photon state as follows:

$$|\Psi\rangle = [C_{00}|00\rangle] + [C_{10}|10\rangle + C_{01}|01\rangle] + [C_{20}|20\rangle + C_{11}|11\rangle + C_{02}|02\rangle] + [C_{30}|30\rangle + C_{21}|21\rangle + C_{12}|12\rangle + C_{03}|03\rangle] + \cdots. \quad (17)$$

Here, each group of terms in square brackets indicates a certain fixed number of total cavity iterations. Thus, the only term in the first square bracket corresponds to both photons emitted together without any intra-cavity reflections. The two terms in the second square bracket correspond to a total number of one cavity iterations between the two photons. The three terms in the third square-bracket correspond to a total number of two cavity iterations between the two photons, and so on for higher-order terms. It can be appreciated from figure 3(a) that all modes within a given square-bracket group involve the same amplitude.

Note that the state in equation (17) exhibits quantum entanglement in the temporal-mode degree of freedom. Note also that the state of each photon is described by a Hilbert space with a dimension of the order of the number of effective cavity round trip times before the state is extinguished. Thus, for a higher coefficient of finesse, there will be more cavity round trip times, and the dimension of the Hilbert space which describes each photon will increase. The triangular shape of the overall pattern of modes (see figure 3(a)) implies that the state is non-factorable. Thus, interestingly, this physical system leads to higher-dimensional entanglement in the temporal-mode degree of freedom with a dimension which can be tailored by adjusting the cavity finesse.

We can carry out a similar analysis for the Cs cavity. The resulting JTI is plotted in figure 3(b). The fact that only one photon is now resonant, implies that the temporal-mode structure now appears only for the signal photon. Note that this state may now be written as $|\Psi\rangle = C_{00}|00\rangle + C_{01}|01\rangle + C_{02}|02\rangle + \cdots$, which is factorable; hence, this system does not lead to entanglement in the temporal-mode degree of freedom.

In order to gain further physical insight into the nature of the two-photon state in the temporal domain, in figure 4(a) we plot the JTI for the same Csi cavity source, this time as a function of the time-sum $t_s + t_i$ and time-difference $t_s - t_i$ variables. Figure 4(b) is similar to the previous plot, except that the state has been spectrally filtered so that only the central spectral mode in the JSI is retained. It may be seen from these plots that the triangular pattern which appears in the latter JTI may be thought of as an "envelope" for the JTI corresponding to the full, i.e. spectrally unfiltered, state. It is interesting to consider the time of arrival difference distribution, which can be obtained from integrating the JTI in panels (a) and (b) over the time-sum variable. The result is plotted in figure 4(e), where the curve composed of multiple peaks corresponds to the spectrally unfiltered state and the other curve, which again may be thought of as an envelope, corresponds to the central peak of the JSI. The multiple peaks visible in the unfiltered time of arrival difference distribution are labeled as $0, \pm1, \pm2, \ldots$ so that a value $j > 0$ means that the signal photon is emitted j cavity iterations *after* the idler photon, whereas a value $j < 0$ means that the signal photon is emitted j cavity iterations *before* the idler photon. The spacing between peaks corresponds to the cavity round trip time.

Figures 4(c), (d) and (f) are similar to panels (a)–(b) and (e), except that they correspond to the Cs cavity source (where the two sources are otherwise identical to each other). Note that in this case the time of arrival difference distribution is asymmetric, where positive values do not occur, i.e. the signal photon in a given pair is always are emitted after the corresponding idler photon.

2.3. Analytical expression in closed form for the joint temporal intensity

As was shown in section 2.2, we can obtain the JTI by numerical evaluation of equation (16). However, in this section we show that it is possible to obtain an expression in closed analytic form under certain approximations.

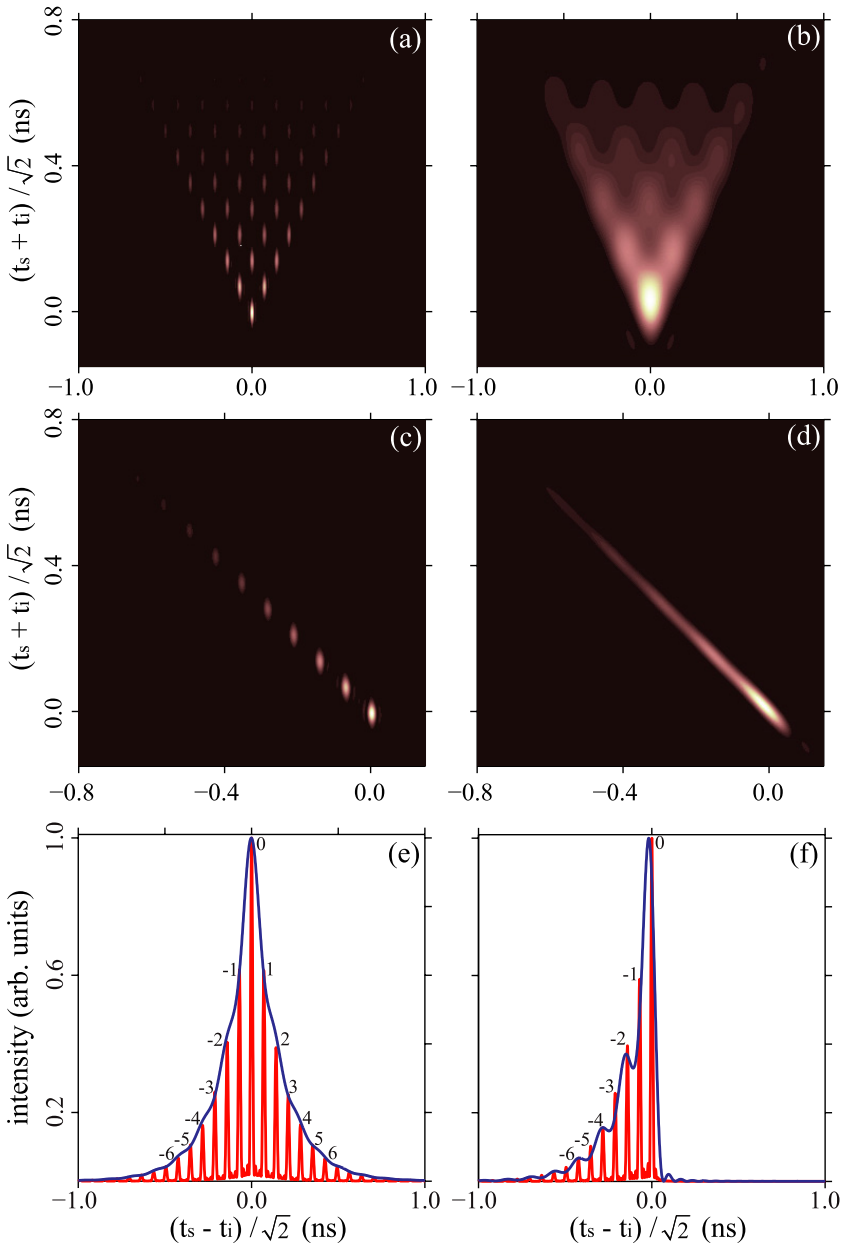

Figure 4. For the same parameters as in figures 2 and 3, panel (a) shows the joint temporal intensity for the Csi cavity plotted as a function of the time-sum $t_s + t_i$ and time-difference $t_s - t_i$ variables. Panel (b) is similar to (a) except that we have assumed that the signal and idler photons are filtered in such a way that a single spectral cavity mode is retained. (e) Represents the time-difference marginal joint temporal intensity, obtained from integrating the joint temporal intensity over the time-sum variable. Note that while the red curve (with distinct peaks) corresponds to panel (a), the blue curve corresponds to panel (b). Panels (c), (d) and (f) are similar to panels (a), (b) and (e), except that the idler-mode resonance has been suppressed (i.e. this corresponds to a Cs cavity).

These approximations include: (i) describing each cavity mode through a Gaussian function of the signal and idler frequencies, (ii) assuming that the SFWM mode widths are equal, i.e. $\delta\omega_s = \delta\omega_i \equiv \delta\omega$, and that the mode spacings are likewise equal, i.e. $\Delta\omega_s = \Delta\omega_i \equiv \Delta\omega$, and (iii) assuming that the JSA can be described only in terms of the pump bandwidth and the cavity mode structure, so that the sinc function in equation (2) can be replaced by unity. Also, let us assume that each of the signal and idler modes is filtered with rectangular spectral filters of width $M\Delta\omega$, centered around the particular cavity mode of interest. Thus, we can write the JSA in the form

$$\Upsilon(\nu_s, \nu_i) = e^{-\frac{(\nu_s+\nu_i)^2}{2\sigma^2}} \sum_{l=-M}^{M} \sum_{m=-M}^{M} e^{-\frac{(\nu_s - l\Delta\omega)^2}{\delta\omega^2}} \times e^{-\frac{(\nu_i - m\Delta\omega)^2}{\delta\omega^2}}, \quad (18)$$

which has been expressed in terms of the frequency detunings $\nu_\mu = \omega_\mu - \omega_{\mu 0}$ (with $\mu = s, i$). The JTA, $\tilde{\Upsilon}(t_s, t_i)$, can now be calculated analytically as the Fourier transform of $\Upsilon(\nu_s, \nu_i)$. It is convenient to express the JTI in terms of the time-sum $t_+ = (t_s + t_i)/\sqrt{2}$ and time-difference $t_- = (t_s - t_i)/\sqrt{2}$

variables, obtaining

$$\tilde{S}_t(t_-, t_+) = \exp\left(-\frac{t_-^2}{\tau_c^2} - \frac{t_+^2}{\tau^2}\right) \times \frac{\sin^2\{(M+\frac{1}{2})\frac{\Delta\omega}{\sqrt{2}}[t_- - \left(\frac{\tau_c}{\tau}\right)^2 t_+]\}}{\sin^2\{\frac{\Delta\omega}{2\sqrt{2}}[t_- - \left(\frac{\tau_c}{\tau}\right)^2 t_+]\}} \times \frac{\sin^2\{(M+\frac{1}{2})\frac{\Delta\omega}{\sqrt{2}}[t_- + \left(\frac{\tau_c}{\tau}\right)^2 t_+]\}}{\sin^2\{\frac{\Delta\omega}{2\sqrt{2}}[t_- + \left(\frac{\tau_c}{\tau}\right)^2 t_+]\}}, \quad (19)$$

In equation (19), $\tau_c = \sqrt{2}/\delta\omega$ is the temporal width along the t_- direction, or correlation time, which defines the uncertainty in the time of emission difference. Note that this parameter is proportional to $\sqrt{\mathscr{F}}$ (see equation (13)), so that increasing the finesse leads to more signal and idler cavity round trips and hence to a greater correlation time. Parameter τ in equation (19), given by $\tau = \tau_c\sqrt{\delta\omega^2 + \sigma^2}/\sigma$, represents the temporal width along the t_+ direction.

3. A specific source design

In this section we wish to present a specific design of a SFWM photon pair cavity source to be used as the basis for an atom–photon interface. Thus, we wish to match the frequency and the emission bandwidth of one of the two SFWM modes, say the signal mode, to an atomic transition. In this example, we will consider as a specific example of an atomic transition the D2 line in cesium which occurs at 852 nm with a bandwidth of $2\pi \times 5.22$ MHz.

Note that appropriate matching of one of the signal SFWM modes to the atomic transition can be accomplished through a Cs cavity, which is resonant only for the signal mode. However, as will be studied in section 4, an important advantage of the Csi cavity versus the Cs (or Ci) cavity, is that it leads to a flux enhancement with respect to the flux attainable in an equivalent source without a cavity. Thus, for the example to be shown here, we will assume that both the signal and idler modes are resonant in the cavity, in other words we will assume that our source is based on a Csi cavity.

As a first step in the design of a suitable SFWM cavity source, a particular fiber geometry must be determined which fulfills phasematching with appropriate pump and idler frequencies so that the signal frequency is precisely matched to the atomic transition. Relying on the step-index model [37] for the description of the dispersion in a PCF, we have found that a PCF with core radius $r = 0.68$ μm and air-filling fraction $f = 0.5$ exhibits phasematching for degenerate pumps at $\lambda_p = 1.064$ μm, with SFWM wavelengths $\lambda_s = 0.852$ μm and $\lambda_i = 1.417$ μm. Note that the λ_s value is matched to the atomic transition. Note also that if the PCF geometry were to be taken into account fully, this would lead to the need for a slight adjustment to the fiber specifications for our choice of frequencies.

The detection of an idler photon at $\lambda_i = 1.417$ μm could herald the presence of a single photon in the signal mode, at $\lambda_s = 0.852$ μm, to interact with the D2 cesium transition. However, note that unless a single cavity mode can be isolated, the heralded photon will contain more than one cavity mode. It is thus necessary to determine a minimum required cavity mode spectral separation so that a single cavity mode may be isolated with existing spectral filters. Using a fiber of length $L = 5$ cm leads (see equation (12)) to a spectral mode separation of $\Delta\omega = 13.5$ GHz, which is many times the mode width $\delta\omega$ and could therefore be isolated from the other modes.

The next step in our source design is to determine the required coefficient of finesse, so as to ensure that the signal photon has a bandwidth which matches that of the atomic transition. Setting the signal-photon bandwidth to $2\pi \times 5.22$ MHz in angular frequency, equation (13) determines the required coefficient of finesse: $\mathscr{F} = 6.2 \times 10^4$ (or a corresponding reflectivity $r_2 = 0.992$).

In figure 5(a) we show a plot of the resulting JSI for our cavity source with the signal mode matched to the D2 line of cesium, where we have assumed a pump bandwidth of $\sigma = 0.1$ THz. In panels (b) and (c) we show the corresponding single-photon spectra for the signal and idler modes. Note that in section 4 we will describe a criterion for selecting the pump bandwidth.

4. Photon pair rate of emission

In this section we focus on the emitted SFWM photon pair flux for a $\chi^{(3)}$ cavity. We define the flux N as the number of photons, say in the signal mode, emitted from the cavity per second. In the case of a pulsed pump, this corresponds to the number of pairs emitted per pump pulse, multiplied by the pump repetition rate R. Thus, for a Csi cavity we obtain the following expression:

$$N = R\sum_k \langle \Psi_2^{si}|\hat{a}^\dagger(k)\hat{a}(k)|\Psi_2^{si}\rangle. \quad (20)$$

By substituting equations (4) and (5) into (20), and following a similar treatment as in [36], which includes writing sums over modes as integrals in the limit $\delta k \to 0$, it can be shown that the emitted flux from a Csi cavity can be expressed as

$$N = \frac{2^5 c^2 n^2(\omega_o) L^2 \gamma^2 p^2}{\pi^3 \omega_o^2 \sigma^2 R} \times \int d\omega_s \int d\omega_i \frac{\omega_s \omega_i k'(\omega_s) k'(\omega_i)}{n^2(\omega_s) n^2(\omega_i)} \mathscr{A}_s(\omega_s)\mathscr{A}_i(\omega_i) \times |f(\omega_s, \omega_i)|^2, \quad (21)$$

where p is the average pump power, $k'(\omega) = dk(\omega)/d\omega$, $\mathscr{A}_\mu(\omega_\mu)$ is given by equation (9), and $f(\omega_s, \omega_i) = (\pi/2)^{1/2}\sigma F(\omega_s, \omega_i)$. Note that this expression for the emitted flux is similar to that obtained for SFWM in the absence of a cavity (see [36]), except for the modified photon pair spectral distribution due to the cavity mode structure.

For the monochromatic pump regime, the SFWM emitted flux is obtained by taking the limit $\sigma \to 0$ of equation (21),

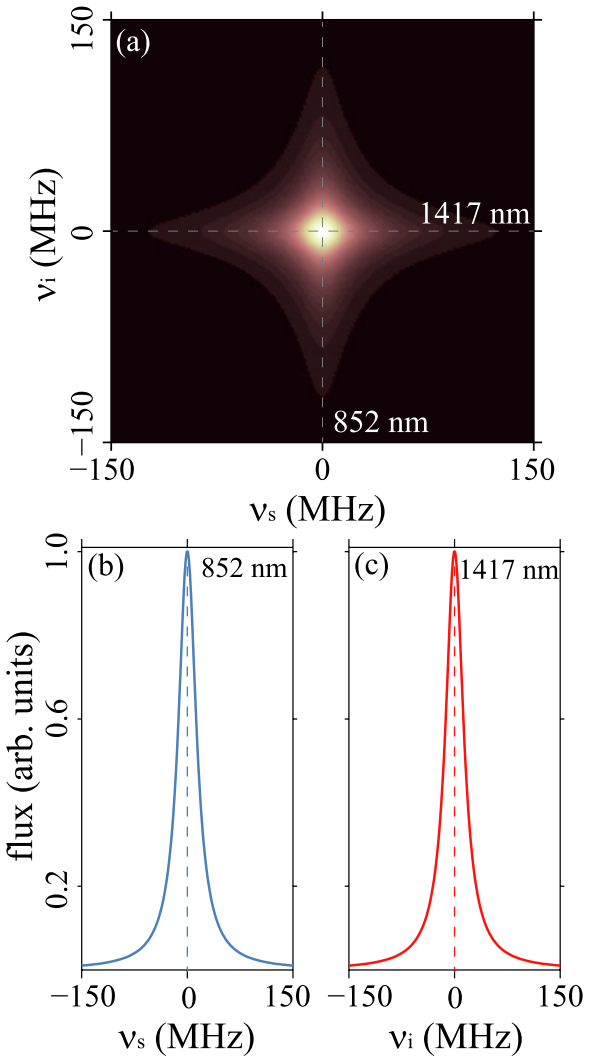

Figure 5. (a) Here we show the joint spectral intensity, plotted as a function of signal and idler frequency detunings, obtained for a specific source design (see text), for which the signal photon has been matched in frequency and bandwidth to the D2 line transition of cesium. (b) Marginal joint spectral distribution for the signal mode obtained by integrating the joint spectral intensity over the idler frequency. (c) Marginal joint spectral distribution for the idler mode obtained by integrating the joint spectral intensity over the signal frequency.

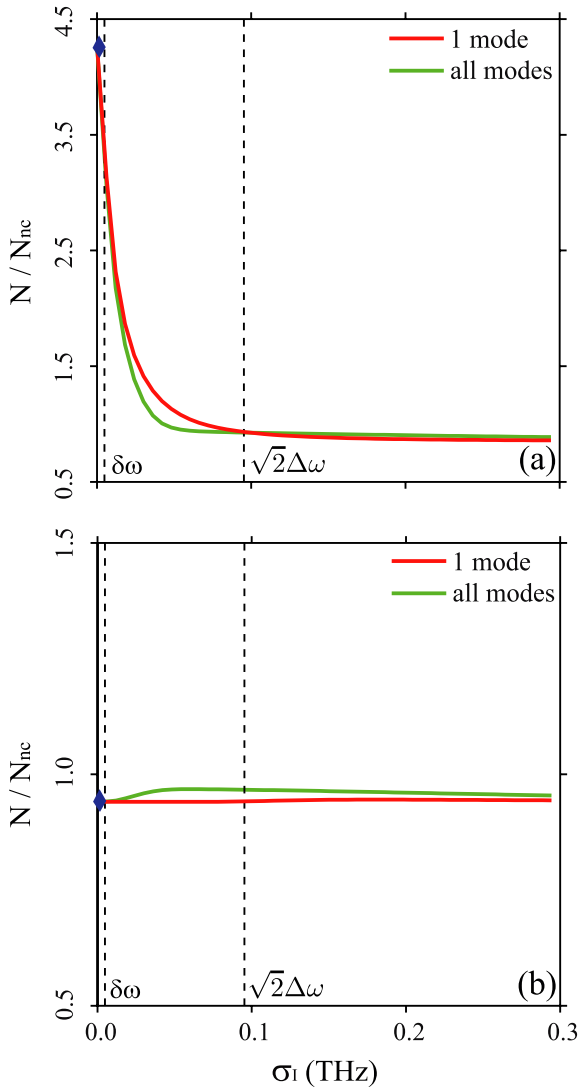

Figure 6. (a) Here we plot $N/N_{\rm nc}$ versus the pump bandwidth $\sigma_{\rm I}$, where N is the SFWM photon pair flux from a Csi cavity source and $N_{\rm nc}$ is the flux of an equivalent source without a cavity. Panel (b) is similar to (a), except that we have suppressed the idler-mode resonance (i.e. we have assumed a Cs cavity).

from which we obtain

$$N_{\rm cw} = \frac{2^5 c^2 n^2(\omega_{\rm p}) L^2 \gamma^2 p^2}{\pi \omega_{\rm p}^2} \times \int {\rm d}\omega \, \frac{\omega(2\omega_{\rm p}-\omega) k'(\omega) k'(2\omega_{\rm p}-\omega)}{n^2(\omega) n^2(2\omega_{\rm p}-\omega)} \times \mathscr{A}_{\rm s}(\omega)\mathscr{A}_{\rm i}(2\omega_{\rm p}-\omega) {\rm sinc}^2[L\Delta k_{\rm cw}/2], \quad (22)$$

where $\omega_{\rm p}$ is the frequency of the monochromatic pump field and the phase mismatch $\Delta k_{\rm cw}$ is given by (see [36])

$$\Delta k_{\rm cw} = 2k(\omega_{\rm p}) - k(\omega) - k(2\omega_{\rm p}-\omega) - 2\gamma p. \quad (23)$$

We are interested in a comparison of the SFWM flux obtained from a cavity source N, based on numerical integration of equation (21), to that obtained from an equivalent source without a cavity, $N_{\rm nc}$, also obtained from equation (21) with $\mathscr{F}_{\rm s} = \mathscr{F}_{\rm i} \to 0$. Note that our numerical results below use the full two-photon state without any approximations. For a numerical comparison, to be presented below, we assume a very similar source configuration as in our specific design presented in section 3. The main difference is that while in the specific design we assumed $r_2 = 0.992$ (or $\mathscr{F} = 6.2 \times 10^4$), here we have assumed $r_2 = 0.8$ (or $\mathscr{F} = 80$). While this lower coefficient of finesse facilitates our numerical calculations, qualitatively the behavior is identical.

In figure 6(a) we show plots of the quantity $N/N_{\rm nc}$ as a function of the pump bandwidth $\sigma_{\rm I}$, where $\sigma_{\rm I} = \sqrt{2\ln(2)}\sigma$ is the intensity FWHM bandwidth of the pump, and while maintaining the average pump power constant. We have shown two curves, one corresponding to spectral filters of widths $5\Delta\omega_{\rm s}$ and $5\Delta\omega_{\rm i}$ present on the paths of the signal and idler photons, so that a total of 25 cavity modes are present in the two-photon state (shown in green), and the

other corresponding to spectral filters $\Delta\omega_s$ and $\Delta\omega_i$, so that a single cavity mode is present (shown in red). It may be appreciated that there is a distinct behavior for each of the three zones: (i) $\sigma_I > \sqrt{2}\Delta\omega$, (ii) $\delta\omega < \sigma_I < \sqrt{2}\Delta\omega$, and (iii) $\sigma_I < \delta\omega$. In the first of these zones, N/N_{nc} is independent of σ_I with a value close to unity. In other words, the flux produced by the cavity is essentially the same as that produced by an equivalent source without a cavity. In the second zone, however, N/N_{nc} rises as σ is reduced until it reaches a maximum value within the third region. The blue diamond shown in figure 6 indicates the flux calculated in the monochromatic pump limit, through numerical integration of equation (22). This behavior implies that for $\sigma_I < \sqrt{2}\Delta\omega'$ there is an enhancement in the flux obtained from the cavity, where the optimum enhancement occurs for small pump bandwidths values, within the region $\sigma_I < \delta\omega$. Note that while the two curves drawn are qualitatively similar to each other, so that the flux enhancement effect occurs in both of these cases, because an atom–photon interface relies on single cavity mode we are more interested in the flux enhancement obtained for a single mode.

Figure 6(b) is similar to figure 6(a), computed for a Cs cavity instead of a Csi cavity. It is interesting to note that in this case N/N_{nc} is close to unity throughout the pump bandwidth range considered. In other words, there is no flux enhancement observed for a SFWM cavity source which is resonant for only one of the two SFWM modes. Thus, in order to observe a flux enhancement, the cavity needs to be resonant for both SFWM photons.

4.1. Flux expressions obtained from a simple geometrical model

The expression which we have derived for the SFWM flux (see equation (21)) is in terms of a two-dimensional integral. While flux values may be obtained through numerical integration of equation (21), as was done for figure 6, we may gain additional physical insight from a crude approximation of the flux as $N = AH$, where A is the area in $\{\omega_s, \omega_i\}$ space in which the joint spectrum has an appreciable magnitude, and H is the maximum value of the joint intensity, within this area. For our present analysis we are interested in the SFWM flux obtained in a $\chi^{(3)}$ cavity, N, normalized by the corresponding flux in an equivalent source without a cavity, likewise expressed as $N_{nc} = A_{nc}H_{nc}$. The quantity ξ may then be approximated as $\xi \approx ad$, where $a \equiv H/H_{nc}$ and $d \equiv A/A_{nc}$.

Because the flux enhancement effect occurs for a single cavity mode in a manner qualitatively similar to that for multiple cavity modes (see figure 6), it is sufficient to analyze the former case in order to obtain an understanding of the relevant physics. Thus, in what follows we study the behavior of ξ as a function of the pump bandwidth, assuming that the signal and idler photons are filtered using rectangular spectral filters of widths $\Delta\omega_s$ and $\Delta\omega_i$, respectively, so that a single cavity mode is retained. Note that while for non-degenerate SFWM the intra-mode spacing $\Delta\omega$ and the mode width $\delta\omega$ differ between the two SFWM modes (for the specific design in section 3 this variation is near 5%), for the present analysis we will assume that $\Delta\omega_s = \Delta\omega_i$ and $\delta\omega_s = \delta\omega_i$. We are interested in the three zones (i) $\sigma_I > \sqrt{2}\Delta\omega$, (ii) $\delta\omega < \sigma_I < \sqrt{2}\Delta\omega$, and (iii) $\sigma_I < \delta\omega$ considered before.

Let us first analyze in this manner a Csi cavity. In this case, it can be shown that parameter a is given by

$$a = \left(\frac{1+|r_2|}{1-|r_2|}\right)^2. \tag{24}$$

In figure 7(a) we show schematically the cavity mode structure. Each circle corresponds to a cavity mode of width $\delta\omega$, separated from each neighboring mode, along the signal and/or idler frequency axes, by $\Delta\omega$. The spectral filters of width $\Delta\omega$ correspond to retaining only the flux produced within one of the squares in the grid shown. The area shaded in red corresponds to the flux emitted with a cavity source, while the (square) area shaded in blue corresponds to the flux emitted with an equivalent source without a cavity.

In region 1, A is the area of a disk of diameter $\delta\omega$, i.e. $A = \pi\delta\omega^2/4$, while A_{nc} is the area of a square of dimension $\Delta\omega$, i.e. $A_{nc} = \Delta\omega^2$, so that

$$\xi_1 = a\frac{\pi\delta\omega^2}{4\Delta\omega^2} = \frac{(1+|r_2|)^2}{4\pi|r_2|}, \tag{25}$$

which is independent of σ_I. In region 2, $A = \pi\delta\omega^2/4$, while $A_{nc} = \sigma_I(\sqrt{2}\Delta\omega - \sigma_I/2)$, so that

$$\xi_2 = \frac{a\pi\delta\omega^2}{4\sigma_I(\sqrt{2}\Delta\omega - \sigma_I/2)}. \tag{26}$$

In region 3, we approximate A as $A \approx \delta\omega\sigma_I$, an approximation which becomes better for smaller σ_I, while $A_{nc} = \sigma_I(\sqrt{2}\Delta\omega - \sigma_I/2)$, so that

$$\xi_3 = \frac{a\delta\omega}{\sqrt{2}\Delta\omega - \sigma_I/2}. \tag{27}$$

Note that the last two expressions for ξ (equations (26) and (27)) depend on σ_I and yield the flux enhancement described below. This leads to an expression for the flux enhancement, E, defined as the quotient ξ_1/ξ_3, with $\sigma_I \to 0$. We thus obtain

$$E = \sqrt{2\mathscr{F}}, \tag{28}$$

making it clear that the flux enhancement increases with the coefficient of finesse.

Let us now turn our attention to a cavity source which is resonant only for one of the SFMW modes, i.e. a Cs or Ci cavity. In this case the parameter a is given by

$$a = \frac{1+|r_2|}{1-|r_2|}. \tag{29}$$

As can be seen in figure 7(b), which is similar to figure 7(a) drawn for the Cs cavity, in all three of the regions considered above, A is the area of a parallelogram with height $\delta\omega$ and base $\sqrt{2}\sigma$, while A_{nc} is also the area of a parallelogram with height $\Delta\omega$ and base $\sqrt{2}\sigma$. Thus, the ratio between the flux emitted from the cavity and the flux emitted from SFWM

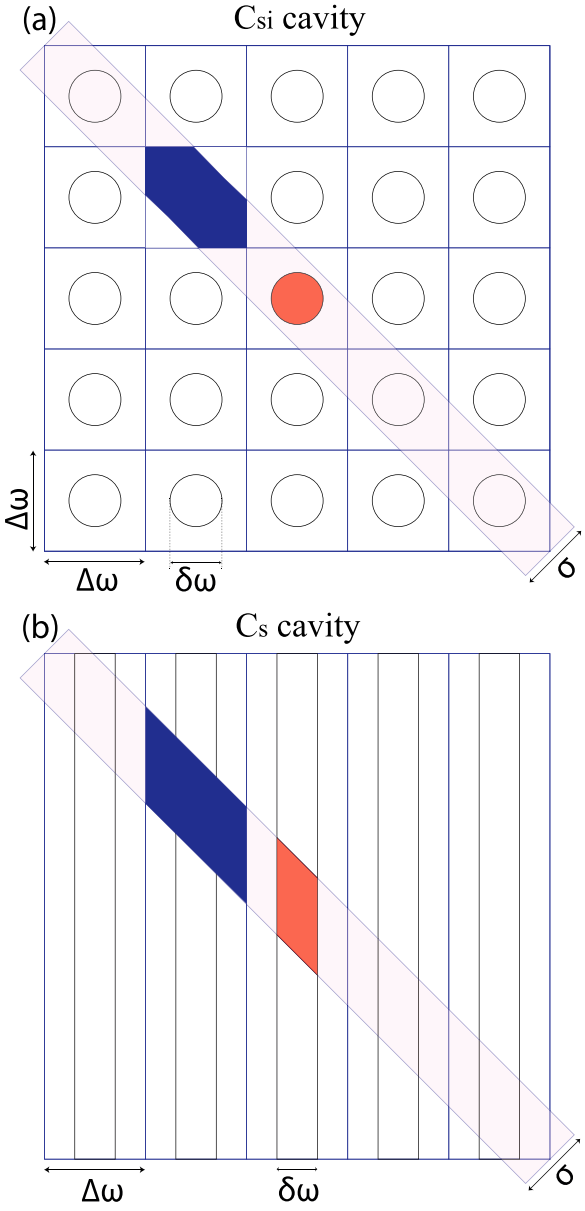

Figure 7. (a) Here we show schematically the mode structure for a Csi cavity in $\{\omega_s, \omega_i\}$ space. Each circle, with diameter $\delta\omega$, represents a spectral cavity mode. The square grid shown has a spacing given by the mode separation $\Delta\omega$, while the diagonal band, with width σ_I indicates the pump spectral amplitude. (b) This panel shows a similar schematic, for a Cs cavity. The cavity modes are now elongated, with a width $\delta\omega$ for the signal mode.

without a cavity is the same in the three regions and is given by

$$\xi = \frac{a\delta\omega}{\Delta\omega}. \tag{30}$$

This result indicates that in a Cs cavity there is no an enhancement in the emitted flux due to the cavity, as was the case for a Csi cavity. This behavior can be appreciated in figure 6.

4.2. Analysis of the absolute efficiency

In our discussion of the SFWM flux, we have so far focused on the flux attainable in a SFWM cavity source relative to

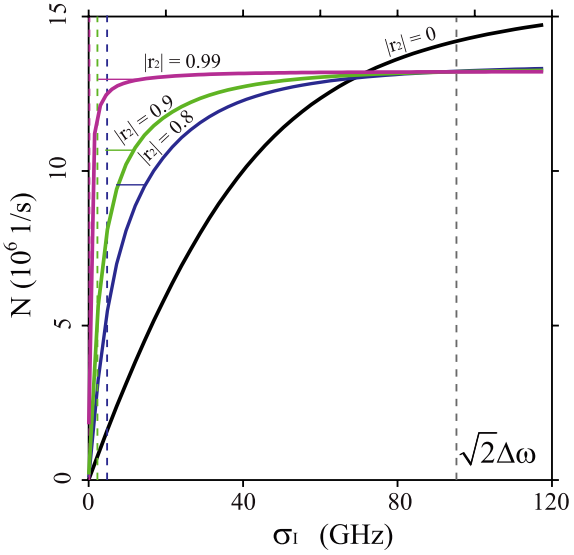

Figure 8. Here we show the absolute flux emitted by a Csi cavity characterized by reflectivities $|r_2| = 0.8, 0.9, 0.99$, with other source parameters selected as for figure 6, as a function of the pump bandwidth σ_I. Also shown is the absolute flux as a function of σ_I for an equivalent source without a cavity. We have indicated with vertical dashed lines the $\delta\omega$ values obtained for each of these three cases, and we have also indicated the $\sqrt{2}\Delta\omega$ value.

an equivalent source without a cavity. It is likewise important to study the flux in absolute terms, which our analysis in section 4 and in particular equation (21) permits.

While much of the behavior of the relative flux discussed so far is qualitatively identical to the behavior expected for a SPDC $\chi^{(2)}$ cavity source, the absolute flux leads to some considerably different behaviors between the $\chi^{(2)}$ and $\chi^{(3)}$ cases. This difference is related to the fact that, for SFWM, two pump photons are annihilated in each generation event rather than just one for SPDC. This implies that, within the phasematching bandwidth σ_{PM} (i.e. for $\sigma_I \lesssim \sigma_{PM}$), the SFWM flux scales linearly with the pump bandwidth σ_I while the SPDC flux remains constant with respect to σ_I for $\sigma_I \lesssim \sigma_{PM}$. In physical terms, each pump frequency of one pump photon may participate in the SFWM process together with all pump frequencies of the other pump photon, limited by phasematching, so that increasing the pump bandwidth leads to a greater range of phasematched frequency combinations, and hence to a greater flux. In contrast, in the case of SPDC, each pump frequency may be considered to act independently from other frequencies leading to a constant flux versus σ dependence, for a constant average pump power.

In figure 8(a) we present the absolute SFWM flux, assuming a Csi cavity, plotted as a function of the pump bandwidth σ_I, for a number of different values of the reflectivity $|r_2|$, in particular for $|r_2| = 0.8$, $|r_2| = 0.9$ and $|r_2| = 0.99$, with other source parameters selected to be identical to those assumed for figure 6. In this figure we have also indicated the cavity mode width $\delta\omega$ value for each of these reflectivities and the $\sqrt{2}\Delta\omega$ value. Note that the effect of the cavity is that the flux versus σ_I dependence is linear for $\sigma_I \lesssim \delta\omega$, climbs more slowly for $\sigma_I \gtrsim \sqrt{2}\delta\omega$, and thereafter

reaches a plateau at a value of σ_I, which for large $\mathscr{F}$ is close to $\delta\omega$. Thus, while the maximum cavity-induced flux enhancement occurs for $\sigma_I \to 0$, as is clear from figure 6, the maximum absolute flux occurs within the above mentioned plateau. For a large $\mathscr{F}$, the flux can be maximized if the pump bandwidth satisfies $\sigma_I \gtrsim \delta\omega$. Note that in the case of Cs cavity, the absolute flux versus σ_I curves (not shown) yield essentially the same curve as the case without cavity shown in figure 8(a).

As a particular example, let us calculate the absolute flux for the specific source design of section 3. This source involves degenerate pumps at $\lambda_p = 1.064$ μm, with SFWM wavelengths $\lambda_s = 0.852$ μm and $\lambda_i = 1.417$ μm. We assume that the cavity source is based on a photonic crystal fiber of length $L = 1$ cm, with a core radius of $r = 0.68$ μm and air-filling fraction of $f = 0.5$. We assume a reflectivity of $|r_2| = 0.998$, which corresponds to a coefficient of finesse of $\mathscr{F} = 9.98 \times 10^5$, and a cavity mode width of $\delta\omega = 2\pi \times 5.22$ MHz, which defines resulting SFWM emission bandwidth and is matched to the D2 line transition of cesium. We assume an average pump power of 300 mW, with a pump bandwidth σ_I selected to have a value $\sigma_I = 5\delta\omega = 0.164$ GHz which fulfils the condition $\sigma_I \gtrsim \delta\omega$ of the previous paragraph. This value of σ_I corresponds to a pulse duration of 16.9 ns, and we assume a repetition rate of 0.1 MHz. The resulting photon pair flux can then determined by numerical integration of equation (21): 1.03×10^9 photon pairs s^{-1}.

5. Conclusions

In this paper we have studied the generation of photon pairs through the process of spontaneous four wave mixing in $\chi^{(3)}$ cavities. We have presented expressions for the two-photon state, showing that in the spectral domain the joint amplitude is given by the product of the corresponding joint amplitude in the absence of a cavity and a matrix of signal and idler modes defined by the cavity. The width of each cavity mode $\delta\omega$ is proportional to $1/\sqrt{\mathscr{F}}$, where $\mathscr{F}$ is the coefficient of finesse. Thus, the emission bandwidth can be effectively controlled by the quality of the cavity, which leads to the possibility of matching the frequency and bandwidth of one of the SFWM photons to a particular atomic transition, for the implementation of photon–atom interfaces.

We have also presented an analysis of the two-photon state in the temporal domain. In particular, we have shown that the spectral cavity modes translate into a corresponding matrix of modes in the temporal domain. The envelope which describes the amplitude of these modes has a non-factorable shape in the space formed by the times of emission. This results in quantum entanglement in the temporal-mode degree of freedom with a dimensionality which scales with the effective number of cavity round trips made by the SFWM photons, as governed by the cavity finesse. Also, we show that by approximating the cavity spectral modes through Gaussian functions it becomes possible to express the joint temporal intensity in closed analytic form.

We have presented expressions for the absolute source brightness, given in terms of a two-dimensional frequency integral. We have evaluated this integral numerically to yield on the one hand a comparison of the flux obtained in the cavity with the flux obtained in an equivalent source without a cavity. Through this analysis we have shown that the use of a pump bandwidth which is smaller than the inter-mode spacing results in a flux enhancement with respect to an equivalent source without a cavity. We have presented a simple geometrical model which clarifies the physics behind the flux enhancement, and leads to an expression for the flux enhancement in terms of the coefficient of finesse. Our analysis on the other hand shows that while the optimum source enhancement occurs for a small pump bandwidth $\sigma_I \to 0$, the absolute source brightness reaches its optimum value, in the case of a large coefficient of finesse, for $\sigma_I \gtrsim \delta\omega$, where $\delta\omega$ is the cavity mode width. We hope that this work will be useful for the implementation of SFWM cavity sources, which could form a crucial component for atom–photon interfaces.

Acknowledgments

This work was supported in part by CONACYT, Mexico, by DGAPA, UNAM and by FONCICYT project 94142.

References

[1] Clark A, Bell B, Fulconis J, Halder M M, Cemlyn B, Alibart O, Xiong C, Wadsworth W J and Rarity J G 2011 *New J. Phys.* **13** 065009
[2] Söller C, Cohen O, Smith B J, Walmsley I A and Silberhorn C 2011 *Phys. Rev.* A **83** 031806
[3] Söller C, Brecht B, Mosley P J, Zang L Y, Podlipensky A, Joly N Y, Russell P St J and Silberhorn C 2010 *Phys. Rev.* A **81** 031801
[4] Halder M, Fulconis J, Cemlyn B, Clark A, Xiong C, Wadsworth W J and Rarity J G 2009 *Opt. Express* **17** 4670–6
[5] Cohen O, Lundeen J S, Smith B J, Puentes G, Mosley P J and Walmsley I A 2009 *Phys. Rev. Lett.* **102** 123603
[6] Garay-Palmett K, McGuinness H J, Cohen O, Lundeen J S, Rangel-Rojo R, Raymer M G, McKinstrie C J, Radic S, U'Ren A B and Walmsley I A 2007 *Opt. Express* **15** 14870
[7] Fan J and Migdall A 2007 *Opt. Express* **15** 2915
[8] Rarity J, Fulconis J, Duligall J, Wadsworth W and Russell P St J 2005 *Opt. Express* **13** 534–44
[9] Fan J, Migdall A and Wang L J 2005 *Opt. Lett.* **30** 3368–70
[10] Medic M, Altepeter J B, Hall M A, Patel M and Kumar P 2010 *Opt. Lett.* **35** 802–4
[11] Fan J, Eisaman M D and Migdall A 2007 *Phys. Rev.* A **76** 043836
[12] Lee K F, Chen J, Liang C, Li X, Voss P L and Kumar P 2006 *Opt. Lett.* **31** 1905–7
[13] Garay-Palmett K, U'Ren A, Rangel-Rojo R, Evans R and Camacho-López S 2008 *Phys. Rev.* A **78** 043827
[14] Ivanin K V, Leontyev A V, Lobkov V S and Samartsev V V 2010 *Laser Phys. Lett.* **7** 583–6
[15] Zamzuri A K, Ismail U S, Al-Mansoori M H, Islam M S and Mahdi M A 2011 *Laser Phys. Lett.* **8** 62–5
[16] Ahmad H, Awang N A, Latif A A, Zulkifli M Z, Ghani Z A and Harun S W 2011 *Laser Phys. Lett.* **8** 742–6
[17] Chen D, Sun B and Wei Y 2010 *Laser Phys.* **20** 1733–7
[18] Sun H B, Liu X M, Wang L R, Li X H and Mao D 2010 *Laser Phys.* **20** 1994–2000
[19] Chen D and Sun B 2011 *Laser Phys.* **21** 919–23
[20] Reim K F, Nunn J, Lorenz V O, Sussman B J, Lee K C, Langford N K, Jaksch D and Walmsley I A 2010 *Nature Photon.* **4** 218–21
[21] Lvovsky A I, Sanders B C and Tittel W 2009 *Nature Photon.* **3** 706–14

[22] Jeronimo-Moreno Y, Rodriguez-Benavides S and U'Ren A B 2010 *Laser Phys.* **20** 1221–33
[23] Ou Z Y and Lu Y J 1999 *Phys. Rev. Lett.* **83** 2556
[24] Raymer M G, Noh J, Banaszek K and Walmsley I A 2005 *Phys. Rev.* A **72** 023825
[25] Kuklewicz C, Wong F and Shapiro J 2006 *Phys. Rev. Lett.* **97** 1–4
[26] Neergaard-Nielsen J S, Nielsen B M, Takahashi H, Vistnes A I and Polzik E S 2007 *Opt. Express* **15** 7940
[27] Bao X-H, Qian Y, Yang J, Zhang H, Chen Z-B, Yang T and Pan J-W 2008 *Phys. Rev. Lett.* **101** 190501
[28] Wang F Y, Shi B S and Guo G C 2008 *Opt. Lett.* **33** 2191–3
[29] Haase A, Piro N, Eschner J and Mitchell M W 2009 *Opt. Lett.* **34** 55
[30] Scholz M, Koch L, Ullmann R and Benson O 2009 *Appl. Phys. Lett.* **94** 201105
[31] Scholz M, Koch L and Benson O 2009 *Phys. Rev. Lett.* **102** 1
[32] Wang F Y, Shi B S and Guo G C 2010 *Opt. Commun.* **283** 2974
[33] Zhang H *et al* 2011 *Nature Photon.* **5** 628
[34] Pomarico E, Sanguinetti B, Osorio C I, Herrmann H and Thew R T 2012 *New J. Phys.* **14** 033008
[35] Clemmen S, Farsi A, Levy J, Helt L, Liscidini M, Sipe J, Lipson M and Gaeta A L 2011 *In Frontiers in Optics, OSA Technical Digest* (Washington, DC: Optical Society of America)
[36] Garay-Palmett K, U'Ren A B and Rangel-Rojo R 2010 *Phys. Rev.* A **82** 043809
[37] Wong G K L, Chen A Y H, Ha S W, Kruhlak R J, Murdoch S G, Leonhardt R, Harvey J D and Joly N Y 2005 *Opt. Express* **13** 8662–70